COMPARISON OF THE CORROSION BEHAVIOUR OF AUSTENITIC STAINLESS STEEL IN SEAWATER AND IN A 3.5 % NaCl SOLUTION

PRIMERJAVA KOROZIJSKIH LASTNOSTI AVSTENITNIH NERJAVNIH JEKEL V MORSKI VODI IN RAZTOPINI S 3,5 % NaCl

Črtomir Donik, Aleksandra Kocijan

Institute of Metals and Technology, Lepi pot 11, 1000 Ljubljana, Slovenia
crtomir.donik@imt.si

The evolution of the passive films on austenitic AISI 316L stainless steel in seawater and in pure 3.5 % NaCl was studied using potentiodynamic (PD) measurements, X-ray photoelectron spectroscopy (XPS) and electrochemical impedance spectroscopy (EIS). This paper describes and evaluates the comparison of pure 3.5 % NaCl with seawater through surface and corrosion measurements. The formation of the passive film was studied by EIS at the open-circuit potential (OCP), by potentiodynamic measurements and by X-ray photoelectron spectroscopy, where their compositions were analysed as a function of depth, and the cationic fraction of the passive film was determined. The passive films on both materials predominantly contained Cr-oxides, whereas the Fe species were markedly depleted.

Keywords: stainless steel, XPS, potentiodynamic measurements, EIS, passivity

Z različnimi tehnikami: z rentgensko fotoelektronsko spektroskopijo (XPS), potenciodinamskimi meritvami (PD) in elektro-kemijsko impedančno spektroskopijo (EIS), smo preučevali rast pasivnih plasti na avstenitnem nerjavnem jeklu AISI 316L v korozijskih medijih: v raztopini 3,5 % NaCl in v morski vodi. Pri EIS-tehniki smo merili tvorbo plasti pri potencialu odprtega kroga (OCP), XPS smo uporabili za analizo tvorjenih plasti na površini v odvisnosti od debeline, medtem ko smo s potenci-odinamskimi meritvami preizkusili osnovne elektrokemijske lastnosti materiala po izpostavitvi v izbranih medijih. Pasivna plast je pri obeh materialih sestavljena iz kromovih oksidov, ki tudi preprečujejo nadaljnjo degradacijo materiala v kloridnem mediju.

Ključne besede: nerjavno jeklo, XPS, potenciodinamske meritve, EIS, pasivacija

1 INTRODUCTION

Stainless steel is one of the most widely used materials and has many different applications in the marine environment, the food industry, households and many other areas. The oxidation and corrosion resistance of austenitic stainless steel have already been the subject of many studies.[1–16] Milošev et al.[10] studied the influence of complexing agents on the formation of a passive layer on the surface of AISI 316L stainless steel. Many of the studies[17–21] use "artificial seawater" or just a higher concentration of NaCl to simulate an environment similar to "real seawater". The corrosion resistance originates from a Cr-rich oxide layer, which works as a barrier against ion diffusion between the alloy and the ambient phase.[22–26] The good corrosion resistance of stainless steel is known to be due to chromium oxide (Cr_2O_3) with a combination of (($Fe, Cr)_2O_3$) at the surface, considered to act as a protective layer against corrosion due to its low diffusion constants for oxygen and metal ions. Abreu et al.[27,28] pointed out the stabilizing effect of molybdenum on the surface of the passive film, enhancing the formation of a layer on austenitic and duplex stainless steel with a higher Cr/Fe ratio. Molybdenum increases the stability of the passive film and, therefore, the ability of the stainless steel to resist localized corrosion, including pitting and crevice corrosion, particularly in environments containing chloride ions. However, the oxide layer formed on stainless-steel surfaces is usually not uniform in terms of depth. Duplex or even triplex layers can be formed on the surface, depending on the alloy composition, the oxidizing conditions (oxidizing atmosphere, time and temperature), the environment of the used stainless steel (marine environment, industrial environment, environment in polluted urban areas, etc.).[1,4,29–31]

AISI 316L is the standard molybdenum-bearing stainless steel, which offers a better overall corrosion resistance than AISI 304L, in particular a higher resistance to pitting and crevice corrosion in chloride solutions.[1,13] In many marine environments they exhibit surface corrosion, which is usually visible as brown staining. This is particularly associated with crevices and a rough surface finish. Compared to chromium–nickel austenitic stainless steels, AISI 316L stainless steel offers higher creep, stress resistance to rupture and tensile strength at elevated temperatures. The aim of this study is a comparison of real seawater immersion, taken from Adriatic Sea, and immersion in pure 3.5 % NaCl.

2 MATERIALS AND METHODS

The composition of the AISI 316 stainless steel in mass fractions was confirmed with analytical chemical methods, as shown in **Table 1**.

Table 1: The composition of the stainless steel AISI 316L (*w*/%)
Tabela 1: Kemijska sestava nerjavnega jekla AISI 316L (*w*/%)

C	Si	Mn	Cr	Ni	P	S	Mo
0.021	0.38	1.4	17.0	10.1	0.041	<0.005	2.1

The concentrations of the elements were determined by using inductively coupled plasma atomic emission spectroscopy (ICP-OES, Agilent 720 instrument). The concentration of carbon was determined by the oxidation of the sample in an induction furnace by heating in an oxygen atmosphere to form CO_2, which was then measured with an infrared detector (Eltra CS-800 instrument). The experiments were carried out in 3.5 % NaCl and seawater from the Adriatic Sea, with a total concentration of chloride ions of 3550 mg/L (approx. 80 % NaCl, with the residual being $MgCl_2$, $CaCl_2$ and others). The density of both solutions was 1.025 g/cm³, and the pH of both tested media was 7.2. All the chemicals were from Merck, Darmstadt, Germany.

The test specimens were cut into discs of diameter 15 mm. The specimens were ground with SiC emery paper down to 4000 grit prior to the electrochemical studies, and then rinsed with distilled water. The specimens were then embedded in a Teflon holder and employed as the working electrode. The reference electrode was a saturated calomel electrode (SCE, 0.242 V vs. SHE) and the counter electrode was flat platinum mesh. All the potentials described in the text are relative to the SCE, unless stated differently.

The potentiodynamic measurements were recorded at room temperature using a BioLogic SP-300 Modular Research Grade Potentiostat/Galvanostat/FRA and EC-LAB software 10.37 computer program. In the case of the potentiodynamic measurements the specimens were immersed in the solution 1 h prior to the measurement in order to stabilize the surface at the OCP. The potentiodynamic curves were recorded, starting at 250 mV (SCE) more negative than the OCP. The potential was then increased, using a scan rate of 1 mV/s, until the transpassive region was reached. A three-electrode flat corrosion cell (volume 0.25 L) was used for the EIS measurements. The test specimen employed was exposed to the solution with an area of 1 cm². A platinum mesh and SSCE electrode were used as the counter and reference electrodes, respectively. The EIS investigations were carried out as well at room temperature using a BioLogic SP-300 Modular Research Grade Potentiostat/Galvanostat/FRA and EC-LAB software 10.37 computer program. The impedance spectra were obtained in the frequency range 65 kHz to 1 mHz, with the amplitude of the excitation signal being 5 mV. The impedance spectra

at the corrosion potential were collected for increasing immersion times (from 1 h to 100 h). The impedance data were interpreted on the basis of equivalent electrical circuits using the ZView version 2.8 program for fitting the experimental data.

The passive layers on the alloy surface were formed at the OCP for 100 h, rinsed with distilled water, dried and transferred to the analyser chamber of the VG Microlab 310F within an hour. The XPS depth profiles of the oxide layers were measured with a VG Microlab 310F AES/SEM/XPS. For all the XPS measurements, Mg K_α radiation at 1253.6 eV with an anode power of 200 W (anode voltage 12.5 kV and emission current 16 mA) was used. A Ar⁺ ion beam 3 keV, 1 μA rastered over a (5 × 4) mm area, was used for the sputter depth profiling with an incidence angle of 60° (measured with respect to the sample normal).[32] The spectra were acquired using the Avantage 3.41v software supplied by the manufacturer. CasaXPS software[33] was used to process the data. The XPS spectra were quantified using the appropriate sensitivity factors and some peaks were separated into their different chemical states using curve fitting. **Figure 1** shows the high-resolution XPS scans of the Cr $2p_{3/2}$ and Fe $2p_{3/2}$ transitions with the corresponding metallic and oxide components before sputtering.

3 RESULTS AND DISCUSSION

The measurements of the potentiodynamic tests are shown in **Figure 2**. The image compares four potentiodynamic curves, which represent four different immersion times: two in 3.5 % NaCl and two in real seawater (after 1 h of stabilization at the open-circuit potential in the solution and after 100 h in the solution). Following the Tafel region all the samples exhibit passive behavior, which ends with the breakdown potential (E_b). The corrosion potentials ($E_{corr.}$) for the studied samples were approximately around –200 mV, just a little higher for the 100 h immersed in 3.5 % NaCl,
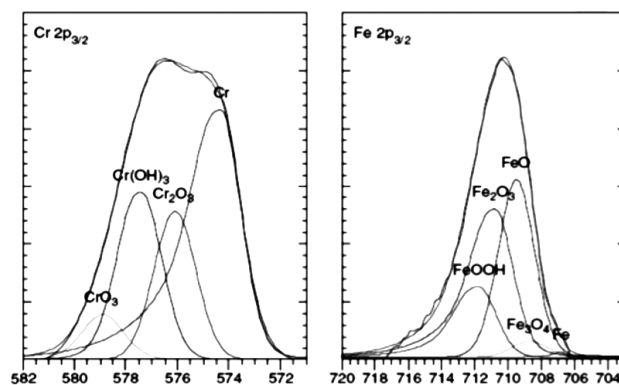

Figure 1: XPS of the Cr $2p_{3/2}$ and Fe $2p_{3/2}$ transitions with the corresponding metallic and oxide components before sputtering used for the XPS depth profiles
Slika 1: XPS-vrhovi Cr $2p_{3/2}$ in Fe $2p_{3/2}$ z označenimi komponentami Feox in Crox, ki smo jih uporabili za izračun globinskih profilov
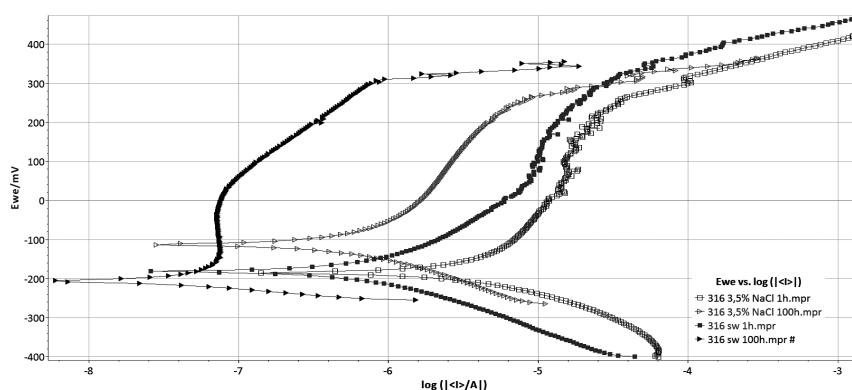
Figure 2: Polarization curves recorded for the AISI 316L in: a) 1 h after being immersed in 3.5 % NaCl, b) after 100 h immersed in 3.5 % NaCl, c) after 1 h immersed in seawater and d) after 100 h immersed in seawater

Slika 2: Polarizacijske krivulje za AISI 316L po: a) enourni izpostavitvi v raztopini 3,5 % NaCl, b) stourni izpostavitvi v raztopini 3,5 % NaCl, c) enourni izpostavitvi v morski vodi in d) stourni izpostavitvi v morski vodi

which shows a slightly narrower passive region than in the case of just one hour immersion in the solution. On the other hand, the E_b values for all the samples were around +300 mV and this confirms the theory that E_b represents the oxidation of water and the transpassive oxidation of the metal species, which in our study were all AISI 316L. From the Tafel region the corrosion current ($i_{corr.}$) can also be calculated (**Table 2**).

Table 2: Calculated $E_{corr.}$ and $i_{corr.}$ from Tafel region

Tabela 2: Izračunani $E_{corr.}$ in $i_{corr.}$ v Tafelovem področju

	3.5 % NaCl, 1 h	3.5 % NaCl, 100 h	Seawater, 1 h	Seawater, 100 h
$E_{corr.}$	–172 mV	–115 mV	–187 mV	–205 mV
$i_{corr.}$	4.071 µA	0.547 µA	0.925 µA	0.022 µA

The calculated $i_{corr.}$ from **Figure 2** shows that the highest is for immersion of 1 h in 3.5 % NaCl, more than four times higher than 1 h immersed in seawater, nevertheless the $E_{corr.}$ is almost identical. The lowest $i_{corr.}$ was measured in the 100 h immersed sample in seawater and it was almost 200 times lower than the 1 h immersed in 3.5 % NaCl. From $i_{corr.}$ it can be calculated with Faraday's law, the corrosion rate, which is directly correlated to $i_{corr.}$ as stated in the equation:

$$v_{corr.} = \frac{EM \cdot i_{corr.}}{F \cdot \rho}$$

where EM is the equivalent weight of the metal divided by the charge number, which indicates the number of electrons exchanged in the dissolution reaction, F is the Faraday constant, (96485 C/mol) and ρ is the density of the alloy. From this equation it was calculated that the corrosion rate in 100 h immersed seawater is $2.5 \cdot 10^{-4}$ mmpy, which means that in seawater in these conditions, without additional oxygen, agitation or diffusion of the solution, 1 mm of this stainless steel would corrode in approximately 4000 years. The interesting artifact is the 100 h immersion in 3.5 % NaCl, which shows a reduction of the $i_{corr.}$, which can be directly

related to the dissolved oxygen ($O_{2(g)}$) in the solution, which increase the $i_{corr.}$ of the alloys.

The open-circuit impedances of the stainless steels 316L was traced over 100 h from the electrode immersion into the 3.5 % NaCl solution and seawater. The effect of the immersion time, the equivalent circuits and the fitted curves for the experimental spectra are presented in **Figure 2** as a Nyquist diagram. The impedance spectra consist of a high-frequency intercept (R_s) with the abscise axis ascribed to the electrolyte's bulk resi-
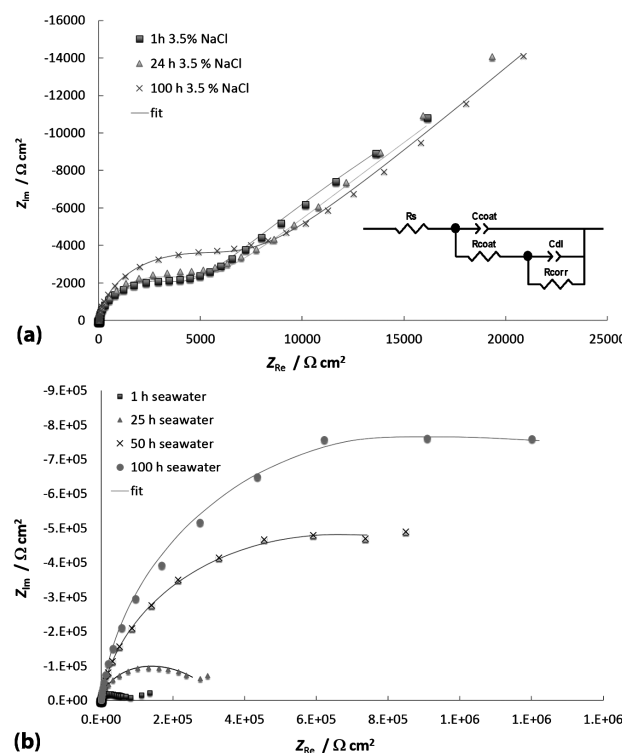

Figure 3: Impedance spectra as a function of immersion time, equivalent circuit and fitted curves of AISI 316L in: a) 3.5 % NaCl and b) seawater, as indicated

Slika 3: Impedančna spektra kot funkcija časa izpostavitve v raztopinah in ekvivalenčno vezje z ujemajočo se krivuljo za nerjavno jeklo AISI 316L v: a) 3,5 % NaCl in b) morski vodi

stance. At lower frequencies, a main arc appears, due to interfacial processes at the metal/electrolyte interface. The interception of this arc with the real axis is ascribed to the polarisation resistance (R_p) and gives a suitable measure for the stability of the passive film. The EIS technique enables us to directly match the electrochemical system under investigation with model circuits consisting of discrete components that are equivalent to the different parameters of the electrochemical system.[34–37] The fitting of the experimental data to the theoretical impedance data leads to the specification of the physical properties of the electrode/electrolyte interface and also to an important mechanistic analysis.[34,38] In the literature there are many different models of interpretation for the impedance spectra on a passive metal surface. In our study we decided to use a model R_s in series with two RQ elements in parallel ($R_1[Q_1(R_2Q_2)]$). This type of model is used and may be viewed as a combination of both the more simple types of models. However, during the process of coverage the film that was already formed may undergo significant changes in its microstructural (thickness, crystallinity) and electrical (resistivity, capacity) properties as well as bio-fouling.

The low-frequency part R_2Q_2 may represent a diffusion phenomenon. MacDonald and co-workers[34,38] proposed the point-defect model, involving the growth and destruction of the passive film. According to this model, the process of migration of the metal vacancies and the oxygen vacancies within the passive film has the form of the Warburg impedance.

The typical generic models were used to fit the impedance data. It was found that the fitting errors of the other models are relatively high or they do not give a reasonable value for the parameter data. The proposed model (**Figure 3**) provided good fits ($\chi^2 < 1 \times 10^{-4}$); however, with an increasing time of immersion, this model results in an order-of-magnitude smaller error of fit.

The impedance spectroscopy shows, in contrast to the other analyses performed in this study, quite a large difference between the samples and or the solutions. From the impedance spectroscopy it can be concluded that a protective film is formed on the surface, which improves the corrosion properties significantly.

Table 3 summarizes all the components used for fitting and quantification of the XPS spectra. Shirley background subtraction was performed. Gaussian-Lorentzian (GL) and asymmetry-modified GL peak shapes were used to fit the measurements. For Cr $2p_{3/2}$, four peaks were used for the fitting: one metallic peak and three oxide peaks, i.e., CrO_3, Cr_2O_3, and $Cr(OH)_3$. The component's binding-energy differences were obtained from the literature[39,40] and the full widths at half maximum (FWHM) for the three oxide peaks were fixed to be the same. The FWHM used for the metallic component was taken from the Cr peak measured after the surface oxides were removed. The three oxides were expected to be present based on previous work.[15,25,26,41] The Fe $2p_{3/2}$ was fitted with five peaks in a similar way.[42,43] The uncertainty ranges of the binding-energy values in **Table 3**

Table 3: List of components corresponding to different elements and their chemical states used for fitting and quantification of the XPS depth profiles with the corresponding binding-energy (*BE*) values
Tabela 3: Tabela kovinskih specij z ustreznimi vezalnimi energijami (*BE*), ki ustrezajo različnim elementom, ki smo jih uporabili za izračun globinskih profilov

component	Fe $2p_{3/2}$	Fe $2p_{3/2}$	Fe $2p_{3/2}$	Fe $2p_{3/2}$	Fe $2p_{3/2}$
	Fe metallic	Fe_2O_3	Fe_3O_4	FeO	FeOOH
BE/eV	707.0 ± 0.2	710.7 ± 0.2	710.0 ± 0.3	708.4 ± 0.3	711.5 ± 0.3
component	Cr $2p_{3/2}$	Cr $2p_{3/2}$	Cr $2p_{3/2}$	Cr $2p_{3/2}$	
	Cr metallic	$Cr(OH)_3$	Cr_2O_3	CrO_3	
BE/eV	574.1 ± 0.1	577.5 ± 0.1	576.1 ± 0.1	578.8 ± 0.2	
component	Mo $3d_{3/2}$	Mo $3d_{3/2}$	Mo $3d_{3/2}$		
	Mo metallic	MoO_2	MoO_3		
BE/eV	230.8 ± 0.1	232.2 ± 0.2	235.2 ± 0.2		
component	Mo $3d_{5/2}$	Mo $3d_{5/2}$	Mo $3d_{5/2}$		
	Mo metallic	MoO_2	MoO_3		
BE/eV	227.7 ± 0.1	229.0 ± 0.2	232.5 ± 0.2		
component	Ni $2p_{3/2}$	Ni $2p_{3/2}$	Ni $2p_{3/2}$		
	Ni metallic	$NiOH_2$	NiO		
BE/eV	853.0 ± 0.2	856.5 ± 0.2	854.5 ± 0.2		
component	O 1s	O 1s			
	O surface	O oxide			
BE/eV	532.0 ± 0.2	530.4 ± 0.2			
component	C 1s				
	C surface				
BE/eV	284.7 ± 0.1				

comprise all the binding-energy values obtained during the fitting process.

The XPS depth profiles are shown in **Figure 4**. In **Figure 4** the metallic and oxide component concentration profiles as well as the oxygen concentration profiles for the samples exposed in different solutions are shown. The stoichiometries of the oxides are approximate, at best, due to ion-sputtering-induced effects, such as the reduction of the oxidation states.[39,44] However, valid comparisons can be made between the relative oxidations. The thickness of the layer can be estimated as 4–5 nm if an effective "half-width" is defined as the sputtering time corresponding to the oxygen concentration being equal to the main bulk metallic component (metallic Fe) concentration multiplied by the estimated sputtering rate. The main oxides are chromium oxides on stainless steels, which can be observed in **Figure 4a**, where Cr-ox is much higher than Fe-ox on the surface, while in **Figure 4b** the Fe-ox is higher on the surface, while after the first sputtering the chromium oxide is increased and is higher than the Fe-ox, after 600 s of sputtering even 3-times higher. This is an interesting observation, since the formation of the oxide layer occurred at room temperature and can be directly connected to the potentiostatic oxidation in solutions. The content of the unoxidized metal species in the topmost part of the

oxide layer is much lower than the content of their oxidized counterparts, while there is virtually no unoxidized chromium or iron in the oxide layer where the layer is in the range of a few nanometers, which is also the range of XPS attenuation lengths for the selected elements. This extremely low thickness of the oxide layer has been corroborated in a separate study[26,44] on a similar sample where thickness estimates obtained from non-destructive angle-dependent XPS and XPS depth profiling were found to agree reasonably well.

The comparison of the depth profiles in **Figures 4a** and **4b** shows that the depth profiles of the immersed samples are very similar, with a slightly different amount of oxygen and carbon on the surface, which is probably due to the bio-fouling of the sample in the seawater.

4 CONCLUSIONS

The results obtained in the present work revealed that the passive film formed on the surface of the AISI 316L in the chloride solutions at pH 7.2 contains oxides of the two main elements, i.e., Cr and Fe as Cr-oxides and Fe-oxides. A slight decrease in the chromium oxide content close to the oxide/solution interface at 100 h exposure in seawater was observed, otherwise the composition of the protective film was comparable between the 3.5 % NaCl and the seawater exposure. However, the electrochemical corrosion tests and the impedance spectroscopy tests show that long-time exposure of the stainless steel AISI 316L differ significantly and should be considered when testing with "artificial" seawater. These differences in the electrochemistry measurement results are probably due to bio-fouling on the surface. This may warrant further investigation.
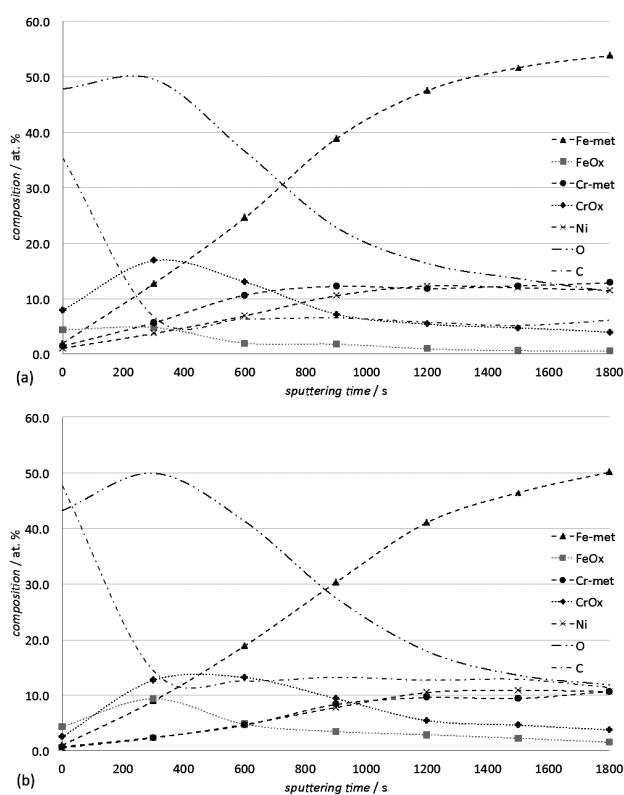

Figure 4: XPS depth profile of the sample immerged 100 h in: a) a 3.5 % NaCl solution at the open-circuit potential, b) same depth profile with immersion in seawater
Slika 4: XPS globinski profil vzorca, izpostavljenega 100 h v: a) raztopini 3,5 % NaCl pri potencialu odprtega kroga in b) v morski vodi

5 REFERENCES

[1] K. H. Lo, C. H. Shek, J. K. L. Lai, Recent developments in stainless steels, Materials Science and Engineering R: Reports, 65 (**2009**), 39–104

[2] H. Asteman, K. Segerdahl, J. E. Svensson, L. G. Johansson, M. Halvarsson, J. E. Tang, Oxidation of Stainless Steel in H_2O/O_2 Environments-Role of Chromium Evaporation, Materials Science Forum, 461–464 (**2004**), 775–782

[3] W. Fredriksson, K. Edstrom, C. A. Olsson, XPS analysis of manganese in stainless steel passive films on 1.4432 and the lean duplex 1.4162, Corrosion Science, 52 (**2010**), 2505–2510

[4] A. Bautista, F. Velasco, S. Guzmán, D. de la Fuente et al., Corrosion behaviour of powder metallurgical stainless steels after two years of exposure in atmosphere, Corrosion Engineering, Science, and Technology, 41 (**2006**), 284–290

[5] J. Gao, Y. Jiang, B. Deng, Z. Ge, J. Li, Determination of pitting initiation of duplex stainless steel using potentiostatic pulse technique, Electrochimica Acta, 55 (**2010**), 4837–4844

[6] A. P. Greeff, C. W. Louw, H. C. Swart, The oxidation of industrial FeCrMo steel, Corrosion Science, 42 (**2000**), 1725–1740

[7] K. Hashimoto, K. Asami, M. Naka, T. Masumoto, Role of alloying elements in improving the corrosion-resistance of amorphous iron base alloys, Corrosion Science, 19 (**1979**), 857–867

⁸ A. Kocijan, Č. Donik, M. Jenko, The corrosion behaviour of duplex stainless steel in chloride solutions studied by XPS, Mater. Tehnol., 43 (**2009**) 4, 195–199

⁹ A. Kocijan, The corrosion behaviour of ferritic stainless steels in alkaline solutions, Mater. Tehnol., 44 (**2010**) 5, 239–242

¹⁰ I. Milosev, H. H. Strehblow, The behavior of stainless steels in physiological solution containing complexing agent studied by X-ray photoelectron spectroscopy, Journal of Biomedical Materials Research, 52 (**2000**), 404–412

¹¹ C. O. A. Olsson, The influence of nitrogen and molybdenum on passive films formed on the austenoferritic stainless-steel-2205 studied by AES and XPS, Corrosion Science, 37 (**1995**), 467–479

¹² C. O. A. Olsson, D. Landolt, Passive films on stainless steels – chemistry, structure and growth, Electrochimica Acta, 48 (**2003**), 1093–1104

¹³ M. Torkar, D. Mandrino, M. Lamut, An AES investigation of brushed AISI 304 stainless steel after corrosion testing, Mater. Tehnol., 42 (**2008**) 1, 39–43

¹⁴ T. Vollmer, P. Gumpel, M. Blaise, W. Racky, Surface treatments and their influence on the corrosion-resistance of stainless-steel, Werkstoffe Und Korrosion-Materials and Corrosion, 46 (**1995**), 92–97

¹⁵ C. Donik et al., Initial oxidation of duplex stainless steel, Applied Surface Science, 255 (**2009**), 7056–7061

¹⁶ D. Mandrino, I. Paulin, S. D. Skapin, Scanning electron microscopy, X-ray diffraction and thermal analysis study of the TiH2 foaming agent, Materials Characterization, 72 (**2012**), 87–93

¹⁷ X. Chang et al., Study of Fe3Al Corrosion Behavior in Simulating Marine Biofilm Environment, Materials And Manufacturing Processes, 25 (**2010**), 302–306

¹⁸ M. da Cunha Belo et al., Chemical composition and semiconducting behaviour of stainless steel passive films in contact with artificial seawater, Corrosion Science, 40 (**1998**), 481–494

¹⁹ J. Duan et al., Corrosion of carbon steel influenced by anaerobic biofilm in natural seawater, Electrochimica Acta, 54 (**2008**), 22–28

²⁰ E. A. M. Hussain, M. J. Robinson, Erosion-corrosion of 2205 duplex stainless steel in flowing seawater containing sand particles, Corrosion Science, 49 (**2007**), 1737–1754

²¹ A. U. Malik, S. Alfozan, Localized corrosion of AISI-316L-S.S in arabian gulf seawater, Desalination, 97 (**1994**), 199–212

²² G. Betz, G. K. Wehner, L. Toth, Composition-vs-depth profiles obtained with auger-electron spectroscopy of air-oxidized stainless-steel surfaces, Journal of Applied Physics, 45 (**1974**), 5312–5316

²³ S. T. Tsai, K. P. Yen, H. C. Shih, The embrittlement of duplex stainless steel in sulfide-containing 3.5 wt% NaCl solution, Corrosion Science, 40 (**1998**), 281–295

²⁴ S. Ohkido, Y. Ishikawa, T. Yoshimura, Applied Surface Science, 76 (**1994**), 261–265

²⁵ C. Donik et al., XPS study of duplex stainless steel oxidized by oxygen atoms, Corrosion Science, 51 (**2009**), 827–832

²⁶ Č. Donik, D. Mandrino, M. Jenko, Depth profiling and angular dependent XPS analysis of ultra thin oxide film on duplex stainless steel, Vacuum, 84 (**2010**), 1266–1269

²⁷ C. M. Abreu et al., Comparative study of passive films of different stainless steels developed on alkaline medium, Electrochimica Acta, 49 (**2004**), 3049–3056

²⁸ C. M. Abreu, M. J. Cristobal, X. R. Novoa, G. Pena, M. C. Perez, Effect of chromium and nitrogen co-implantation on the characteristics of the passive layer developed on austenitic and duplex stainless steels, Surface and Interface Analysis, 40 (**2008**), 294–298

²⁹ A. Vesel et al., AES investigation of the stainless steel surface oxidized in plasma, Vacuum, 82 (**2008**), 228–231

³⁰ A. Vesel, M. Mozetic, A. Drenik, N. Hauptman, M. Balat-Pichelin, High temperature oxidation of stainless steel AISI 316L in air plasma, Applied Surface Science, 255 (**2008**), 1759–1765

³¹ S. Tang, O. J. Kwon, N. Lu, H. S. Choi, Surface characteristics of AISI 304L stainless steel after an atmospheric pressure plasma treatment, Surface & Coatings Technology, 195 (**2005**), 298–306

³² N. S. McIntyre, F. W. Stanchell, Preferential sputtering in oxides as metals and revealed by X-ray photoelectron-spectroscopy, Journal of Vacuum Science & Technology, 16 (**1979**), 798–802

³³ N. Fairley, CasaXPS VAMAS Processing Software, http://www.casaxps.com/

³⁴ D. D. MacDonald, S. Real, S. I. Smedley, M. Urquidi-MacDonald, Evaluation of alloy anodes for aluminum-air batteries. IV, Electrochemical impedance analysis of pure aluminum in 4M KOH at 25 °C, Journal of the Electrochemical Society, 135 (**1988**), 2410–2414

³⁵ F. Mansfeld, S. Lin, S. Kim, H. Shih, Electrochemical impedance spectroscopy as a monitoring tool for passivation and localized corrosion of aluminum alloys, Werkstoffe und Korrosion, 39 (**1988**), 487–492

³⁶ J. F. McCann, S. P. S. Badwal, Equivalent circuit analysis of the impedance response of semiconductor/electrolyte/counterelectrode cells, Journal of the Electrochemical Society, 129 (**1982**), 551–559

³⁷ S. H. Song, P. Xiao, An impedance spectroscopy study of oxide films formed during high temperature oxidation of an austenitic stainless steel, Journal of Materials Science, 38 (**2003**), 499–506

³⁸ N. Bonanos, B. C. H. Steele, E. P. Butler, D. D. MacDonald, M. C. H. McKubre, In: E. Barsoukov, J. R. Macdonald (Eds.), Impedance Spectroscopy: Theory, Experiment, and Applications, chap. 4, 2ⁿᵈ ed., John Wiley & Sons Inc., Hoboken, NJ 2005

³⁹ C. Leygraf, G. Hultquis, S. Ekelund, J. C. Eriksson, Surface composition studies of (100) and (110) faces of monocrystalline Fe84Cr16, Surface Science, 46 (**1974**), 157–176

⁴⁰ C. Leygraf, G. Hultquist, Initial oxidation stages on Fe-Cr(100) and Fe-Cr(110) surfaces, Surface Science, 61 (**1976**), 69–84

⁴¹ Č. Donik, A. Kocijan, I. Paulin, M. Jenko, The oxidation of duplex stainless steel at moderately elevated temperatures, Mater. Tehnol., 43 (**2009**) 3, 137–142

⁴² S. Swaminathan, M. Spiegel, Effect of alloy composition on the selective oxidation of ternary Fe-Si-Cr, Fe-Mn-Cr model alloys, Surface and Interface Analysis, 40 (**2008**), 268–272

⁴³ L. Milošev et al., Extensive metallosis and necrosis in failed prostheses with cemented titanium-alloy stems and ceramic heads, Journal of Bone and Joint Surgery-British, 82B (**2000**), 352–357

⁴⁴ I. Saeki et al., The effect of the oxidation atmosphere on the initial oxidation of type 430 stainless steel at 1273 K, Corrosion Science, 40 (**1998**), 191–200